# Accepted Manuscript


Stabilizing the body centered cubic crystal in titanium alloys by a nano-scale concentration modulation

H.L. Wang, S.A.A. Shah, Y.L. Hao, F. Prima, T. Li, J.M. Cairney, Y.D. Wang, Y. Wang, E.G. Obbard, S.J. Li, R. Yang

PII: S0925-8388(16)34335-3

DOI: 10.1016/j.jallcom.2016.12.406

Reference: JALCOM 40329

To appear in: *Journal of Alloys and Compounds*

Received Date: 22 September 2016

Revised Date: 26 December 2016

Accepted Date: 29 December 2016

Please cite this article as: H.L. Wang, S.A.A. Shah, Y.L. Hao, F. Prima, T. Li, J.M. Cairney, Y.D. Wang, Y. Wang, E.G. Obbard, S.J. Li, R. Yang, Stabilizing the body centered cubic crystal in titanium alloys by a nano-scale concentration modulation, *Journal of Alloys and Compounds* (2017), doi: 10.1016/j.jallcom.2016.12.406.

# Graphical abstract

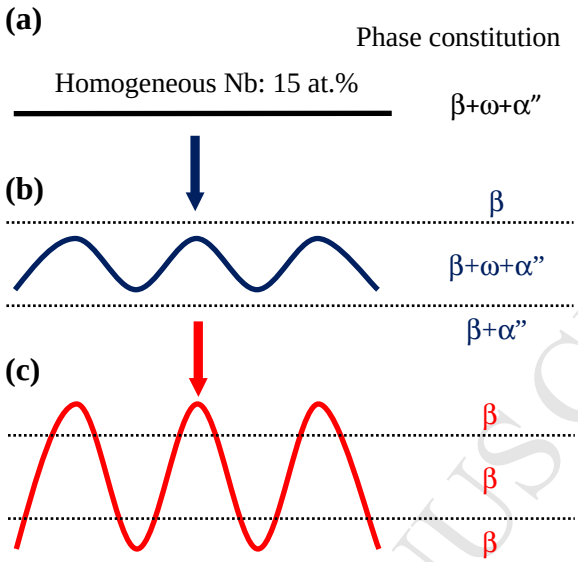

# Stabilizing the body centered cubic crystal in titanium alloys by a nano-scale concentration modulation

H.L. Wang,[1] S.A.A. Shah,[1] Y.L. Hao,[1*] F. Prima,[2] T. Li,[3,4] J.M. Cairney,[3,4] Y.D. Wang,[5] Y. Wang,[6,7] E.G. Obbard,[8] S.J. Li,[1] R. Yang[1]

[1] Shenyang National Laboratory for Materials Science, Institute of Metal Research, Chinese Academy of Sciences, 72 Wenhua Road, Shenyang 110016, China
[2] PSL Research University, Chimie ParisTech–CNS, Institu de Recherche de Chimie Paris, Paris 75005, France
[3] School of Aerospace, Mechanical & Mechatronic Engineering, University of Sydney, Sydney, NSW 2006, Australia
[4] Australian Centre for Microscopy and Microanalysis, University of Sydney, Sydney, NSW 2006, Australia
[5] State Key Laboratory for Advanced Metals and Materials, University of Science and Technology Beijing, Beijing 100083, China
[6] State Key Laboratory for Mechanical Behavior of Materials and Frontier Institute of Science and Technology, Xi'an Jiaotong University, Xi'an 710049, China,
[7] Department of Materials Science and Engineering, Ohio State University, Columbus, OH 43210, USA
[8] Department of Electrical Engineering and Telecommunications, University of New South Wales, Sydney, NSW 2052, Australia

**Abstract**

It is well-known that the body centered cubic (bcc) crystal in titanium alloys reaches its stability limit as the electron-to-atom ($e/a$) ratio of the alloy drops down to ~4.24. This critical value, however, is much higher than that of a multifunctional bcc type alloy ($e/a$ = 4.15). Here we demonstrate that a nano-scale concentration modulation created by spinodal decomposition is what stabilizes the bcc crystal of the alloy. Aided by such a nano-scale concentration heterogeneity, unexpected properties from its chemically homogeneous counterpart are obtained. This provides a new strategy to design functional titanium alloys by tuning the spinodal decomposition.

Keywords: Titanium alloys; Composition fluctuation; Crystal structure; Synchrotron radiation; Shape memory; Elasticity.

[*] Corresponding author. Tel: 86-24-83978841; Fax: 86-24-23972021.
E-mail address: ylhao@imr.ac.cn.

## 1. Introdution

With decreasing stability, some physical and mechanical properties of a phase vary monotonically till its stability limit. To achieve desired properties, some alloys have been designed close to this limit. For example, the bcc β phase in titanium alloys reaches the limit at the electron-to-atom (*e*/*a*) ratio of ~4.24 [1]. Aimed at this critical value, several groups of metastable β-type titanium alloys have been developed, including low modulus alloys for orthopedic applications that alleviate the "stress shielding" effect [2-4], multifunctional alloys that display superelasticity and tunable thermal expansion across a wide temperature range together with high strength, low modulus and good ductility [5-8], and Ni-free shape memory alloys for biomedical applications that have the potential to replace NiTi alloys for eliminating the allergic effect due to the released Ni ions [9-12].

The above alloy design strategy is demonstrated by Fig. 1 where the modulus of the β phase decreases almost linearly as its stability (measured by the *e*/*a* ratio [1]) decreases through the reduction of β stabilizers. The tendency is broken at *e*/*a* ratio of ~4.24, corresponding to ~24Nb in at.% and ~36Nb in wt.%, respectively, in Ti-Nb binary system, due to the formation of ω phase and/or the α" martensite as the alloys are quenched from the high temperature β phase field. There is a modulus peak near the *e*/*a* ratio of ~4.15, corresponding to ~15Nb in at.% and ~24Nb in wt.%. Examples of Ti-Nb based alloys developed near the *e*/*a* ratio of ~4.24 [2-5], include the low modulus biomedical alloys such as Ti-29Nb-13Ta-4.6Zr and Ti-35Nb-5Ta-7Zr (both in wt.%) and the multifunctional alloys such as the Gum Metals (typically Ti-24Nb (at.%) or Ti-36Nb (wt.%) based alloys).

On the other hand, both superelasticity and shape memory effect, which are induced by a reversible martensitic transformation (MT) to the α" martensite [1], also vary linearly with the *e*/*a* ratio because the MT strain is larger with lower *e*/*a* ratio [12,13]. Extending the relation to Ti-rich end, the maximum MT strain could be over ~10% [8,12], which is higher than that of the typical NiTi alloys. Such large strain, however, cannot be utilized because one cannot suppress the α phase formation near the MT starting temperature (*M*s), which is over 1000 K [12,13]. To stabilize the β

phase, most alloys developed so far have high *e*/*a* ratio in general. Correspondingly, their superelasticity is less than 3% [14].

The above demonstration reveals that the β phase with lower *e*/*a* ratio the merits of lower modulus and larger MT strain. Now, the question remains how to stabilize the β phase under the condition of low *e*/*a* ratio. Previous studies have shown that the quenching induced phase transformations are fully suppressed in an alloy with the *e*/*a* ratio of 4.15 by the addition of both Zr and Sn [6,13], which are neutral elements in titanium alloys due to their weak effect on the β transus temperature ($T_\beta$) [1]. The alloy has a composition of Ti-24Nb-4Zr-8Sn in wt.% and Ti-15Nb-2.5Zr-4Sn in at.%, which is abbreviated as Ti2448 from its composition in wt.% [15]. Due to its low *e*/*a* ratio of 4.15, the alloy has lower modulus than the previous alloys, which have a ratio of 4.24. Here we use a <100> orientated single crystal that exhibits almost a linear elasticity, which is suitable for accurate modulus measurement. The data showed that the <100> crystal of Ti2448 has modulus of 27 GPa whereas that of Gum Metal is 40 GPa [16,17], 50% higher than the former.

Therefore, Ti2448 should be a model alloy to explore the origin of the enhanced phase stability. Recently, a nano-scale Nb concentration modulation generated by spinodal decomposition was detected by 3D atomic probe tomography (APT) analysis. This structure is believe to be responsible for some unprecedented properties such as superelasticity from ≤4.2 K up to 500 K and fully tunable thermal expansion (from positive, through zero, to negative) from ≤4.2 K up to 625 K [18]. Here we focus on the nano-scale modulated Nb and its stabilizing effect on the β phase, in hope of revealing the origin of the stable bcc phase at low *e*/*a* ratio. Additionally, both the modulus and the superelasticity of the alloy are estimated by using the concept of composite materials and the results are compared with the experimental data.

## 2. Material and methods

An ingot of Ti2448 alloy with a diameter of 380 mm was fabricated by vacuum arc melting by using a Ti-Sn master alloy and pure Ti, Nb and Zr as raw materials. The ingot has actual compositions of 24.2Nb, 3.94Zr, 8.18Sn and 0.12O, which were obtained by wet chemical and gas analyses. It was hot-forged at 1123 K to form round

bars 55 mm in diameter and then hot-rolled at 1073 K to 12 mm in diameter. Microstructural analysis was conducted on a JEOL 200 CX-II TEM operated at 200 kV. The TEM specimens were prepared by electrolytic thinning in a solution with 60 ml perchloric acid, 85 ml n-butanol and 150 ml methanol at ~240 K. The synchrotron X-ray diffraction (SXRD) analysis was performed on beamline ID-11-C at Advanced Photon Source (APS), Argonne National Laboratory (ANL) using 113 keV x-ray with a wavelength of 0.0112 nm and beam size of 250 $\mu m^2$. A 1.5 mm thick band shaped sample was exposed with the longitudinal axis perpendicular to the X-ray beam. Diffraction patterns were collected by a 2D digital detector.

## 3. Results and discussion

The hot-rolled alloy has a deformed microstructure with an average grain size of ~5 μm [19]. TEM analysis found that the alloy has a fine microstructure with ~0.6 μm features (Fig. 2a), termed as subgrains because the misorientation angels are generally less than 2 degrees. The selected area diffraction (SAD) analysis at ~300 K showed a single β phase microstructure and neither the α″ martensite nor the ω phase can be detected (inset in Fig. 2a). The 2D SXRD profiles measured at 400 K and 110 K fail to detect the thermally induced metastable phase transformations to the α″ martensite and the ω phase (Fig. 2b). These results are in agreement with the previous reports [15-20].

The recent 3D APT analyses revealed that the alloy passes through a spinodal decomposition [18]. This creates a compositional non-uniformity at the nano-scale, consisting of periodically distributed Nb-rich and Nb-lean domains that are 2~3 nm in size and approximately equiaxed (Fig. 2c). The Nb contents range between ~8 at.% and ~22 at.% with an average of 15.1 at.%, approaching the nominal Nb of the alloy. This nano-scale Nb modulation results in smearing of the metastable phase transformations. As shown in Fig. 1, the ω phase reaches its maximum volume fraction at the location of the $e/a$ ratio = 4.15, the origin for the modulus peak. When the Nb concentration deviates from this critical point, the modulus goes down due to the ω phase suppression. This reveals that, for an alloy with the $e/a$ ratio of 4.15, the occurrence of Nb modulation favors to suppress the ω phase in a manner that the

stronger the Nb modulation the less the ω phase.

A schematic is shown in Fig. 3 to demonstrate the Nb modulation in Ti2448 alloy and its suppression of the ω phase. Assuming a homogeneous Nb of 15 at.% (Fig. 3a), the alloy should have a β+ω+α" three-phase microstructure. As the separation occurs (Fig. 3b), the alloy should contain fewer ω phase due to the deviation of Nb from 15 at.%. This tendency becomes stronger with the enhanced Nb separation. As the local Nb content is out of the upper and the lower limits of the ω phase formation (noted by two dash lines in Fig. 3), the alloy should contain three periodical microstructures in turn with the decreased Nb, namely: the single β phase (Nb above the upper limit), the β+ω+α" three-phase and the β+α" two-phase (Nb below the lower limit). Thus, the adjacent Nb-rich and Nb-lean regions create a barrier for the ω nucleation and growth in the middle region. For the Nb modulation with the size of 2~3 nm observed in the alloy [18], the middle region is too small to nucleate the ω phase. This leads to a full suppression of the ω phase (Fig. 3c).

Coupling with the ω phase suppression by the nano-scale Nb modulation (Fig. 3), the MT in the Nb-lean domain can also be controlled by the Nb-rich domain because the former is less stable than the later, as evidenced by that the *M*s decreases linearly with the increase of Nb [12]. Thus, the MT in the Nb-lean region is confined by a pair of its surrounding Nb-rich domains. With the evolution of the modulation, the Nb-rich region can be elastic stable. This creates an elastic confinement to against the MT in the Nb-lean region. This explains the previous findings that the MT in the alloy is solely stress-induced rather than both thermal- and stress- induced in the typical shape memory alloys [18,20,21].

Since the Nb domains in the alloy keep bcc crystal structure, some properties can be estimated roughly from the average results of the β phase in which the Nb ranges from ~8 at.% to ~22 at.%. Such simplification is correct for the modulus (Fig. 4a). To present the advantage of Nb modulation on the modulus softening, a Ti-24Nb (wt.%) binary alloy, which has an identical $T_\beta$ of ~1000 K with Ti2448 [8], is given in Fig. 4a. It is clear that the combined additions of the neutral elements Zr and Sn in Ti-24Nb suppress the transformations to both the ω phase and the α" martensite. As a result,

Ti2448 has a modulus just half of that in Ti-24Nb (Fig. 4a).

Theoretically, the reversible deformation of the alloy cannot be estimated by the averaged MT strains as we do in Fig. 4a for the average modulus. This is because the nano-scale Nb-rich framework is elastic stable and the Nb-lean inclusion favors the MT. Thus, the stress-induced reversibility of the alloy must be coupled by the elastic deformation of the former and the MT strain of the later. Such simplification, however, looks to be reasonable for the maximum superelasticity (SE), which is ~4.5% at 77 K (Fig. 4b) [18]. If adding the total recovery strain, SE+SM, of ~5.5% at 77 K into Fig. 4b, the value is higher than the average of ~4.5%.

It should be noted that the modulations of Zr, Sn and O were observed from the APT data but their modulations locate mainly in the range of experimental error [18]. Thus, their distributions are assumed to be homogeneous in Ti2448 alloy, which has a low *e*/*a* ratio of 4.15. This is different with the previous findings in the alloys with a large ratio of ~4.24 [22,23].

## 4. Conclusion

In summary, the concentration modulation created by the spinodal decomposition is a valid way to stabilize the bcc crystal. These novel properties of Ti2448 alloy such as low modulus, large recovery, high strength and tunable thermal expansion would be improved further by optimizing the Nb modulation. Additionally, several kinds of phase separations and the induced modulation of the β stabilizers have been observed in many β type titanium alloys [22-29]. If these separations were isostructural like in Ti2448, novel properties would also be obtained.

**Acknowledgements**

We thank the supportt from MOST of China (2015AA033702, 2016YFC1102600), NSF of China (51571190, 51271180, 51527801) and NSF of U.S. (DMR-1410322). Use of the Advanced Photon Source was supported by U.S. Department of Energy under Contract No. DE-AC02-06CH11357.

[1] E.W. Collings, Physical metallurgy of titanium alloys. Metals Park, OH: ASM; 1984.

[2] M. Long, H.J. Rack, Biomaterials (19) 1998 1621.

[3] M. Niinomi, Metall. Mater. Trans. A 33 (2002) 477.

[4] Y.L. Hao, M. Niinomi, D. Kuroda, K. Fukunaga, Y.L. Zhou, R. Yang, A. Suzuki, Metall. Mater. Trans. A 33 (2002) 3137.

[5] T. Saito, T. Furuta, J.H. Hwang, S. Kuramoto, K. Nishino, N. Suzuki, R. Chen, A. Yamada, K. Ito, Y. Seno, T. Nonaka, H. Ikehata, N. Nagasako, C. Iwamoto, Y. Ikuhara, T. Sakuma, Science 300 (2003) 464.

[6] Y.L. Hao, S.J. Li, S.Y. Sun, C.Y. Zheng, Q.M. Hu, R. Yang, Appl. Phys. Lett. 87 (2005) 091906.

[7] M. Abdel-Hady, H. Fuwa, K. Hinoshita, H. Kimura, Y. Shinzato, M. Morinaga, Scripta Mater. 57 (2007) 1000.

[8] Y.L. Hao, S.J. Li, F. Prima, R. Yang, Scripta Mater. 67 (2012) 487.

[9] T. Grosdidier, M.J. Philippe, Mater. Sci. Eng. A 291 (2000) 218.

[10] E. Takahashi, T. Sakurai, S. Watanabe, N. Masahashi, S. Hanada, Mater. Trans. 43 (2002) 2978.

[11] S. Miyazaki, H.Y. Kim, H. Hosoda, Mater. Sci. Eng. A 438-440 (2006) 18.

[12] H.Y. Kim, Y. Ikehara, J.I. Kim, H. Hosoda, S. Miyazaki, Acta Mater. 54 (2006) 2419.

[13] Y.L. Hao, S.J. Li, S.Y. Sun, R. Yang, Mater. Sci. Eng. A 441 (2006) 112.

[14] L.L. Pavon, H.Y. Kim, H. Hosoda, S. Miyazaki, Scripta Mater. 95 (2015) 46.

[15] Y.L. Hao, S.J. Li, S.Y. Sun, C.Y. Zheng, R. Yang, Acta Biomater. 3 (2007) 277.

[16] N. Takesue, Y. Shimizu, T. Yano, M. Hara, S. Kuramoto, J. Crystal Growth 311 (2009) 3319.

[17] Y.W. Zhang, S.J. Li, E.G. Obbard, H. Wang, S.C. Wang, Y.L. Hao, R. Yang, Acta Mater. 59 (2011) 3081.

[18] Y.L. Hao, H.L. Wang, T. Li, J.M. Cairney, A.V. Ceguerra, Y.D. Wang, Y. Wang, D. Wang, E.G. Obbard, S.J. Li, R. Yang, J. Mater. Sci. Tech. (2016) doi: 10.1016/ j.jmst.2016.06.017.

[19] S.Q. Zhang, S.J. Li, M.T. Jia, F. Prima, L.J. Chen, Y.L. Hao, R. Yang, Acta Mater. 59 (2011) 4690.

[20] E.G. Obbard, Y.L. Hao, R.J. Talling, S.J. Li, Y.W. Zhang, D. Dye, R. Yang, Acta Mater. 59 (2011) 112.

[21] J.P. Liu, Y.D. Wang, Y.L. Hao, Y.Z. Wang, Z.H. Nie, D. Wang, Y. Ren, Z.P. Lu, J.G. Wang, H.L. Wang, X.D. Hui, N. Lu, M.J. Kim, R. Yang, Sci. Rep. 3 (2013) 2156.

[22] M. Tahara, H.Y. Kim, T. Inamura, H. Hosoda, S. Miyazaki, Acta Mater. 59 (2011) 6208.

[23] Y.F. Zheng, D. Banerjee, H.L. Frazer, Scripta Mater. 116 (2016) 131.

[24] S.L. Saas, J. Less Common Met. 28 (1972) 157.

[25] T. Furuhara, T. Makino, Y. Idei, H. Ishigaki, A. Takada, T. Maki, Mater. Trans. 39 (1998) 31.

[26] N.G. Jones, R.J. Dashwood, M. Tackson, D. Dye, Acta Mater. 57 (2009) 3830.

[27] P. Barriobero-Vila, G. Requena, F. Warchomicka, A. Stark, N. Schell, T. Buslaps, J. Mater. Sci. 50 (2015) 1412.

[28] Y.M. Zhu, S.M. Zhu, M.S. Pargusch, J.F. Nie, Scripta Mater. 112 (2016) 46.

[29] Y.F. Zheng, R.E.A. Willianms, H.L. Frazer, Scripta Mater. 113 (2016) 202.

# Captions of Figures

Fig. 1 Variation of elastic modulus with the *e*/*a* ratio of Ti-Nb based alloys, in which the red curve notes the design strategy of Ti2448 alloy [15].

Fig. 2 The single β phase Ti2448 alloy confirmed by (a) TEM microstructure and the SAD pattern analyzed at ~300 K and (b) 1D SXRD profiles measured at 400 K and 110 K, which integrated from 2D profiles, and its nano-scale Nb modulation shown by (c) 2D APT image of Nb distribution.

Fig. 3 The nano-scale Nb modulation and its stabilization on the bcc β phase: the schematics in (a-c) show the evolution of Nb modulation and the corresponding phase constitutions, in which the dash lines note the upper and lower limits for the ω phase formation in Ti-Nb-2.5Zr-4Sn (at.%) system [13].

Fig. 4 Both the elastic modulus (a) and the recovery strain (b) of Ti2448 alloy at the *e*/*a* ratio of 4.15. The dash lines note that the bcc β phase with lower *e*/*a* ratio exhibits lower modulus (a) and larger MT strain (b), which are extrapolated from the data in Ti-Nb-Zr-Sn quaternary system [8,13].

Figure 1

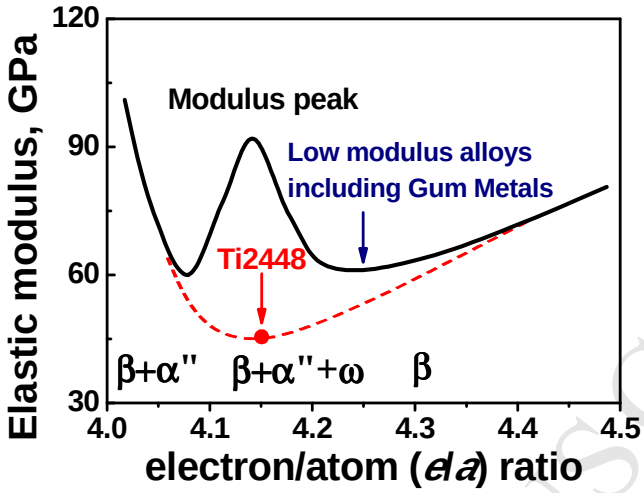

Figure 2

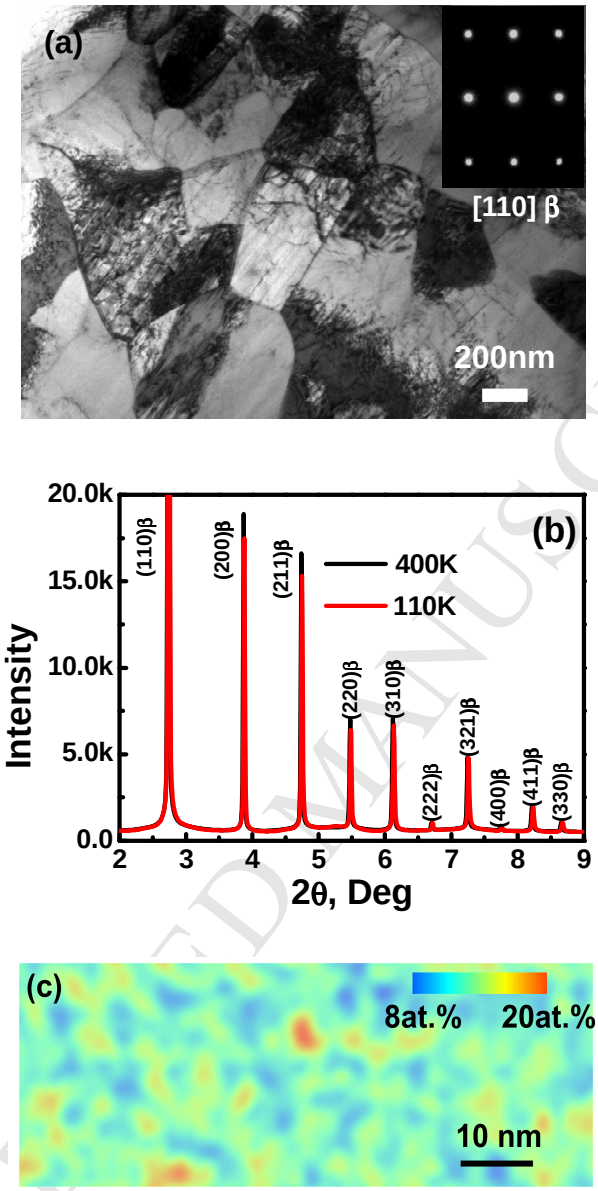

Figure 3

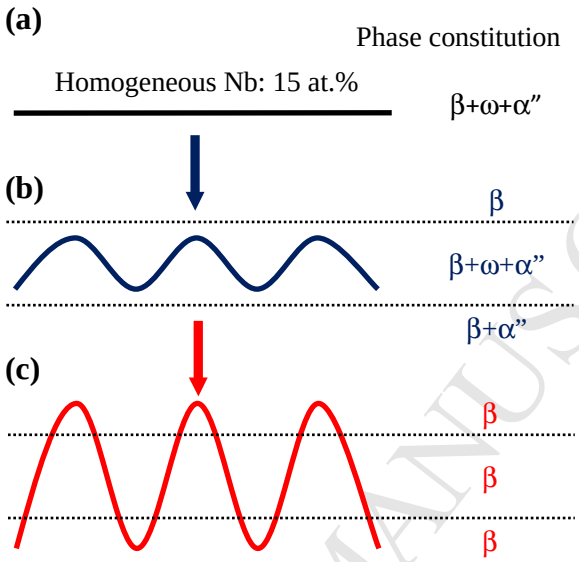

Figure 4